Oxidation of Metals, Vol. 55, Nos. 1/2, 2001

High-Temperature Oxidation and Corrosion of Structural Materials in Molten Chlorides

J. E. Indacochea,* J. L. Smith,* K. R. Litko,* E. J. Karell,* and A. G. Raraz*

Received June 21, 1999; revised July, 21 2000

A molten salt-based process for treatment of spent oxide fuels is under development at the Argonne National Laboratory. A major part of the development effort involves identification of corrosion-resistant structural materials for the process vessels. Coupons of two stainless steels, tantalum, and two Inconel alloys were submitted to a corrosion test in an argon atmosphere with 10% oxygen. The coupons were partially immersed in molten lithium chloride salt containing small amounts of lithium metal, lithium oxide, and lithium nitride. Two sets of coupons were tested, the first at 750°C for 30 days and the second at 650°C for 6 days. Coupons of the first set corroded completely. In the second set of coupons, all corroded to some extent, but Inconel 600 showed the best performance overall. The salt-exposed region generally showed the greatest corrosion in the other coupons. One of the 316L SS coupons was welded and the weld area was severely attacked.

KEY WORDS: High temperature; oxidation; corrosion; molten chlorides.

INTRODUCTION

A new technology is being developed for treatment of spent uranium-oxide based nuclear fuels for durable geologic disposal.[1] This technique involves reduction of the spent oxide fuel with lithium chloride saturated with lithium metal at temperatures of 650–725°C. A concern for the full-scale implementation of this technique is the durability of the material to be used in constructing the vessel. The structural vessel material must be able to

*Chemical Technology Division, Argonne National Laboratory, Argonne, Illinois 60439.

0030-770X/01/0200-0001$19.50/0

resist the harsh molten-salt environments encountered in these pyrometallurgical treatments. This environment consists of molten lithium chloride that contains small quantities of lithium metal, lithium oxide, and lithium nitride.

In this investigation, we attempted to reproduce the conditions that exist during this pyrometallurgical treatment of the spent fuel. The objective is to investigate the role of the different salt constituents in the corrosion of the vessel materials when oxygen is present in the cover gas. In earlier research,[2] corrosion tests were performed in LiC1–Li_2O–Li_3N under an argon cover gas that was free of oxygen. Metal coupons of tantalum and of ferrous alloys were exposed to the salt at 725°C for 30 days. Results from that work showed no corrosion. It was concluded that, in an argon environment, lithium and oxygen ions in the presence of chlorides do not lead to corrosion of structural metals. For the investigation reported in this publication, the corrosion experiment was carried out at a lower temperature, 650°C, in an atmosphere of argon containing oxygen. The molten salt did not contain Li_3N.

Corrosion and passivation of metals in molten-salt environments have been previously investigated, but no technical report has considered a complex system such as the one used in this work. Some salt systems containing only chlorides have been reviewed, with lithium chloride among them.[3] The strong oxidizing conditions in corrosion by molten salts have also been pointed out.[4] Few studies have been conducted on the corrosion behavior of metals in oxide-containing molten-salt electrolytes. Some measurements have been made in fused sulfates[5] and nitrates.[6] Inman and Weaver[7] and Takahashi *et al.*[8] studied the formation of oxide films on platinum. Feng and Melendres[9] studied the electrochemical behavior of iron, nickel, cobalt, copper, and molybdenum in molten LiC1–KCl eutectic containing lithium and oxygen ions at 375°C and 450°C. The current-potential curves obtained exhibited characteristic corrosion–passivation behavior similar to that found in aqueous systems. Feng and Melendres found that the anodic corrosion rates were considerably lower than for metals in pure LiCl—KCl.

Rahmel[10] has reviewed the corrosion of iron- and nickel-base alloys in chloride melts. He indicated that, in the presence of air, the corrosion resistance of steels is related to the high chromium and nickel content. On the other hand, the corrosion rate of nickel-based alloys is proportional to the oxygen partial pressure. The effects of chlorine gas on the high-temperature oxidation of iron and steels have been previously studied.[11–16] The most striking effect in these studies is the rapid response of the corrosion phenomena upon the introduction of the chloride-containing contamination into the environment. Researchers have reported that as soon as sodium chloride is introduced as a vapor into the oxidizing atmosphere or as grains onto the

oxide scale of the steel, the oxidation is strongly accelerated.[12,13] In thermogravimetric studies, an immediate increase of the oxidation rate was observed upon introduction of HCl into the gas flow or upon deposition of some NaCl on to the preoxidized sample.[15,16] Birks and Meier[17] have inferred to the induction of catastrophic attack in iron- and nickel-base alloys by the refractory metals present in these alloys.

A procedure that has been suggested to improve the corrosion performance of alloy steels is to aluminize the metal surfaces.[10] When aluminized rotor shafts in gas turbines were exposed to temperatures of 800 to 850°C, it was found that the scale resistance of the steel rotor blades improved greatly.[18] In our investigation, some of the 316L stainless steel coupons were aluminized to check the corrosion performance in an environment containing molten chlorides.

EXPERIMENTAL WORK

The salt initially used for these corrosion tests under oxidizing conditions consisted of LiCl with 3.5 wt.% Li_2O and 1 wt.% Li_3N. The Li_3N was later omitted as described below. Two sets of metallic coupons were tested. The first set was comprised of the same materials used in the previous study,[2] namely, tantalum, 316L stainless steel, 422 stainless steel (12% Cr, 1% Mo, V, and W), 430 stainless steel, and $2\frac{1}{4}$ Cr–1% Mo steel. The second set of coupons, which was tested under slightly different conditions, was comprised of 304 stainless steel, 316L stainless steel (two coupons), Inconel 600, and Inconel 625. Both 316L stainless-steel coupons had an autogeneous gas tungsten arc-weld pass along the center of the coupon. One of these coupons was also aluminized after welding. The idea was to test the influence of different contents of chromium and nickel and the presence of some refractory metals in the composition of both stainless steels and Inconel alloys. The compositions of the alloys are presented in Table I. The samples

Table I. Compositions of Materials Used in Electrochemical Corrosion Tests for Six Days at 650°C

	Composition (wt.%)					
Sample ID	Fe	Cr	Ni	Mo	C	Others
304 SS	Bal.	18–20	8–10.5	—	0.08	Mn, Si, P, S
316L SS-w[a]	Bal.	16–18	10–14	2–3	0.03	Mn, Si, P, S
316L SS-w-Al[a]	Bal.	16–18	10–14	2–3	0.03	Mn, Si, P, S
Inconel 600	8	15.5	76	—	0.08	Mn, Si, Cu, S
Inconel 625	2.5	21.5	61	9	0.05	Mn, Si, Al, Nb, Ta, S

[a]In the 316L SS sample, the "w" means welded; the "w-Al" means welded and aluminized.

were 1-in. wide, about 0.12-in. thick, and 3-in. long (25.4 mm × 3.0 mm × 76.2 mm). Welded specimens were tested for the purpose of investigating the corrosion performance of dissimilar microstructures in the same coupon. The welded samples were tested in the molten salt under two conditions: after welding and after heat treating. Prior to corrosion testing, the specimens were cleaned thoroughly and weighed, and their thickness measured at several locations.

The corrosion test for the first set of specimens was conducted at a temperature of 725°C in a gas atmosphere of argon with 10% oxygen. This gas was also bubbled through the molten salt. The corrosion test for the second set of test samples was carried out in a similar salt without Li_3N. The test temperature for the second test was also lower, 650°C, but the gas atmosphere, argon with 10% oxygen, was the same and gas also bubbled through the molten salt. During testing, all samples were partially submerged in the molten salt, so that part of each sample was exposed to gas only.

All coupons were visually inspected after the corrosion test and the salt attached to the test samples was removed by washing with deionized water in an ultrasonic cleaner. The insoluble part of the corrosion scale removed from the coupons was analyzed using X-ray diffraction (XRD). All clean coupons were later checked for changes in thickness and weight and subsequently examined by optical and scanning-electron microscopy (SEM). Selected spots in corroded samples were analyzed by energy-dispersive spectrometry (EDS).

RESULTS AND DISCUSSION

The first set of specimens, which were tested for 30 days at 725°C, corroded so completely that the coupons disappeared. Even the stainless-steel rods used for hanging the coupons corroded extensively. There were no specimens left on which to perform a metallurgical characterization. These results reflected the severity of the environment and prompted adjustments in the corrosion test conditions for subsequent testing. In succeeding corrosion tests, the salt mixture did not contain Li_3N but was otherwise unchanged (LiCl with 3.5 wt.% Li_2O). The temperature was reduced to 650°C and the time was shortened to 6 days. The dimensions of these test specimens differed from those in the first corrosion test. Table II presents the results of the second set of tests.

Corrosion of Stainless-Steel Specimens

The corrosion layer attached to some test coupons was tenacious. Sometimes it took several washings to remove most of the scale and, even

Table II. Corrosion Results of 6-Day Test of Coupons in Oxidizing Conditions, at 650°C[a]

Sample ID	Weight before test (gm)	Weight after test (gm)	Weight loss (%)	Thickness before test (mm)	Thickness after test (mm)	Thickness reduction (salt region) (mm)
304 SS	91.9357	77.843	15.33	6.230	6.030	0.200
316L SS-w	45.9983	39.7717	13.54	3.177	3.070	0.107 (Weld)
				3.027	2.930	0.097 (Base metal)
316L SS-w-Al	45.4847	40.2638	11.48	3.169	2.940	0.229 (Weld)
				3.030	2.803	0.227 (Base metal)
Inconel 600	39.0218	38.1652	2.2	3.271	3.240	0.031
Inconel 625	25.7473	11.2371	56.36	1.601	0.977	0.624

[a]See footnote to Table I.

then, small patches still remained attached to some test coupons, for example, the 304 SS coupon. That sample exhibited the second highest percentage weight loss (Table II). However, the weight loss would have been even higher had the corrosion scale been removed completely. The 316L SS specimens, despite their molybdenum content, did not appear to perform differently than the 304 SS samples, since the weight loss in both types of coupons was similar. Nevertheless, the corrosion resistance of these two steels can be differentiated by considering the reduction of their thicknesses. The reduction was smallest for bare 316L SS, slightly greater for 304 SS, and greatest for aluminized 316L SS (0.097, 0.200, and 0.220 mm, respectively). The larger decrease in the aluminized 316L SS sample must be due to the disappearance of the aluminum coating. The thickness of the as-deposited aluminum layer was measured metallographically to be about 100 μm. At first, it was speculated that the aluminum had dissolved in the molten salt. However, no aluminum was found in the gas-exposed region of the coupon either, so dissolution was ruled out. Metallographic examination of the aluminized sample before testing revealed a poor aluminum deposit with lack of a metallurgical bond and significant interfacial porosity (Fig. 1). Little interdiffusion had occurred between the steel and the aluminum. It is possible that aluminum oxidized and detached from the stainless steel substrate early in the test. This supposition is consistent with the difference between the thermal-expansion coefficients of the stainless steel and the aluminum oxide: 17.5 μm/m °C for the 316L SS and 8.5 μm/m °C for Al_2O_3 (at about 600°C).[19,20]

The coupons were partially immersed and thus exposed to three environments: salt, salt/gas, and gas. The corrosion performance of each coupon was evaluated in each of the three regions. Figure 2 illustrates the extent of corrosion in each region of one coupon. All stainless-steel coupons showed

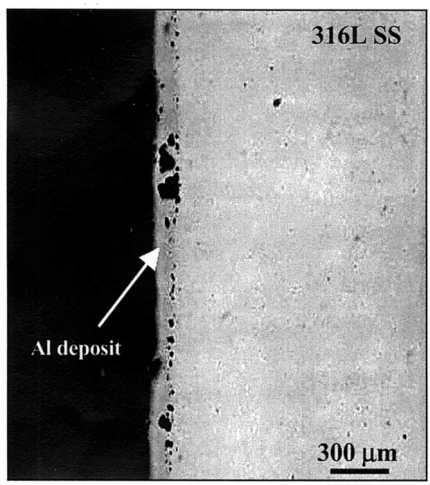

Fig. 1. Optical micrograph of as-received 316L stainless steel that had been commercially aluminized.

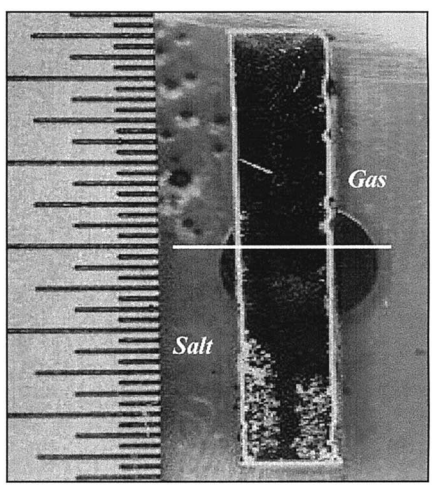

Fig. 2. Cross section along gas–salt interface. Corrosion localized in salt region. Aluminized 316L SS after 6-day electrochemical corrosion.

attack, and the portion of the coupon exposed to the salt showed the most severe corrosion. In the portion of the welded coupon (316L SS-w) that was exposed to the molten chloride, the weld metal was found to have corroded extensively (Fig. 3a), but in addition, significant intergranular corrosion attack was observed in the heat-affected zone and base metal (Fig. 3b). Intergranular attack was observed in this 316L SS sample despite its low levels of carbon. The 316 SS composition has been considered as an alternative to 316L for structural use because it has improved creep properties, which are due, in large part, to its higher carbon content. However, the

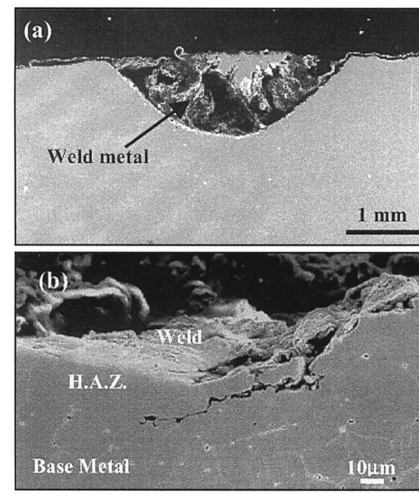

Fig. 3. Welded 316L SS coupon after 6-day corrosion at 650°C. (a) Corrosion of weld metal and (b) intergranular corrosion of the heat-affected zone (H.A.Z.) and base metal.

higher carbon content should cause the steel to be more susceptible to sensitization at this operating temperature and, thus, more prone to intergranular corrosion.

The corrosion product left from ultrasonic cleaning of the 316L SS was analyzed by XRD; the results are given in Table III, which also lists the primary components of the corrosion product obtained from washing the welded and aluminized 316L SS coupon. Figure 4a shows the cross section of the portion of the welded and aluminized 316L SS coupon that was exposed to the salt; it reveals no aluminum at the surface. The test coupon had a thin corrosion layer attached to it at some locations. Figure 4a, from the same micrograph, shows serious intergranular corrosion underneath the corrosion layer and, in spots, grain pullout as well. The corrosion layer is nonuniform and porous (Fig. 4b). Observations at higher magnifications of this corrosion band revealed some dense layers (Fig. 5). The EDS spot-chemical analyses of the corrosion layers shown in Fig. 5 are given in Table

Table III. Corrosion Products Identified by XRD[a]

Sample ID	Compounds
304 SS	CrO, Fe_3O_4, Fe_2O_3, $NiFe_2O_4$, and $NiCr_2O_4$
316L SS-w-Al	CrO, Cr_2O_3, Fe_3O_4, Fe_2O_3, $FeCr_2O_4$, and $NiFe_2O_4$
316L SS-w	CrO, NiO, FeO, Fe_2O_3, $FeCr_2O_4$, $NiFe_2O_4$, and trace Al_2O_3
Inconel 600	NiO, $LiFeO_2$, and $LiCrO_2$
Inconel 625	Ni, $FeNi_3$, Fe_3O_4, $NiFe_2O_4$, $Li_2Ni_8O_{10}$, and $LiFO_2$

[a]See footnote to Table I.

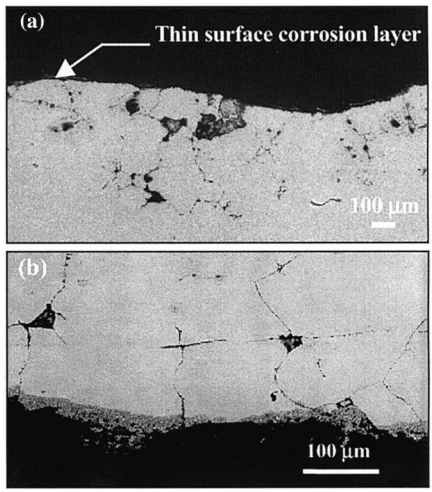

Fig. 4. Aluminized 316L SS coupon after 6-day corrosion at 650°C. Salt exposed area: (a) surface free of aluminum and (b) porous corrosion layer and intergranular corrosion.

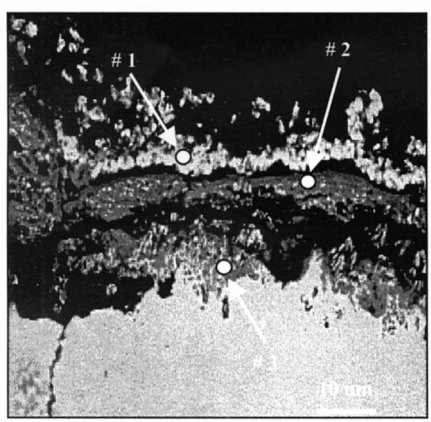

Fig. 5. Corrosion layer of welded and aluminized 316L SS after 6-day corrosion at 650°C. Region exposed to salt. Spots are the locations of EDS analyses.

IV. The light porous corrosion layer of the outer surface (spot #1, Fig. 5) was found to be rich in Ni (76.6 wt.%); the dark-gray layer (spot #2, Fig. 5) was denser and was determined to be rich in Cr (51.8 wt.%). There was just a trace of Al at the porous layer (<1 wt.%) and no Al in the denser corrosion layer. As indicated above, the Al had not diffused into the stainless-steel substrate and no metallurgical bonding was produced. This made it difficult to evaluate whether Al improved the corrosion resistance.

The migration of Ni to the outer corrosion layer could have been influenced by the tendency of Ni, Fe, and Al to form solid solutions between

Table IV. Spot Chemical Analysis by EDS

Sample ID	Location/standard	Elemental content (wt.%)				
		Cr	Fe	Ni	Mo	Al
316L SS-w-Al	Standard	16–18	68.5	10–14	—	—
(Fig. 5)	Spot #1	6.0	16.0	77.0	—	< 1.0
	Spot #2	52.0	27.5	15.0	—	—
Inconel 600	Standard	15.5	8.0	76.0	—	—
(Fig. 9)	Substrate	13.8	8.7	77.4	—	—
	Spot #1	35.0	27.0	37.5	—	—
	Spot #2	4.0	2.0	94.0	—	—
	Spot #3	2.0	1.0	97.0	—	—
Inconel 625	Standard	21.5	2.5	61.0	—	—
(Fig. 11a)	Substrate	21.7	2.8	75.0	—	—
	Spot #1	2.0	12.0	86.0	—	—
	Spot #2	83.0	5.0	12.0	—	—
	Spot #3	1.0	0.0	95.0	—	—
	Spot #4	9.0	2.0	87.0	—	—

aluminides. Studies on the aluminum corner of the aluminum–iron–nickel system,[21] report that $FeNiAl_9$ and $FeNiAl_{10}$ are created and that compounds of NiAl and FeAl form a continuous series of solid solutions between themselves. Investigations of the aluminum–iron–chromium system rich in aluminum[22] showed no ternary compounds in this system.

Corrosion of Inconel Samples

Inconel 600 showed the best corrosion resistance among the samples tested in this investigation. Table II shows a weight loss of about 2% and a total thickness reduction of about 30 μm for this specimen. Surprisingly, the Inconel 625 coupon had a serious reduction in mass, one-half of its original weight, and a significant decrease in thickness. As seen in Fig. 6, rounding of this coupon edges was observed in the cross sections from both the gas- and salt-exposed regions. The two Inconels have similar composition, except that the Inconel 625 contains molybdenum, more chromium, and less iron. The presence of molybdenum could make Inconel 625 more susceptible to corrosion as explained by Birks and Meier.[17]

The corrosion behavior of Inconel 600 was similar in both the salt and gas regions (Fig. 7). The corrosion scale attached to the substrate was thin. This scale was not easily found in those samples cross sectioned from the salt region. Presumably, the scale broke off during cooling as a result of residual stresses, since the coefficients of thermal expansion of the substrate,

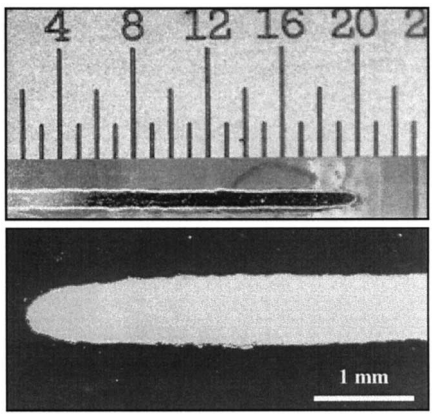

Fig. 6. Inconel 625 coupon after 6-day corrosion at 650°C. Photographs illustrate the rounding of the coupon edges.

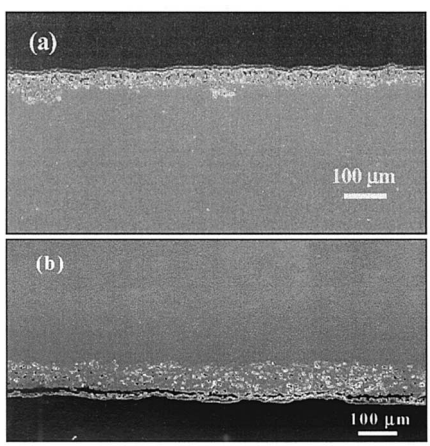

Fig. 7. Inconel 600 coupon after 6-day corrosion at 650°C. (a) Salt-exposed and (b) gas-exposed area.

the corrosion layer, and the salt attached to it are different. In the gas-exposed region, however, this corrosion scale was found attached to the test coupon (Fig. 7b). It was noticed that corrosion was in progress nonetheless underneath the surface corrosion scale (Fig. 7b). The corrosion type for this sample appears to be corrosion pitting, with no intergranular attack (Fig. 8). This corrosion zone had a depth of 60 to 125 μm in the Inconel-600 coupon. A spot-chemical analysis of the corrosion scale and adjacent substrate region was carried out with EDS, as illustrated in Fig. 9, the information is given in Table IV. These chemical results indicate a surface-corrosion scale rich in chromium and iron. The composition as identified by XRD is given in Table III.

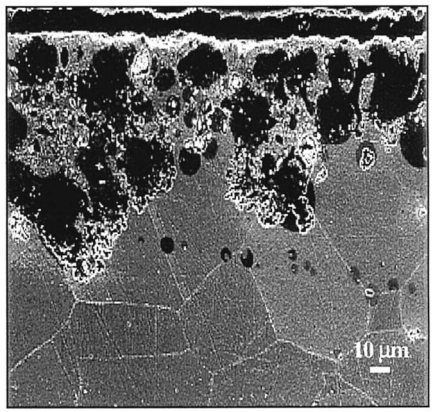

Fig. 8. Inconel 600 coupon after 6-day corrosion test at 650°C. Region exposed to molten salt.

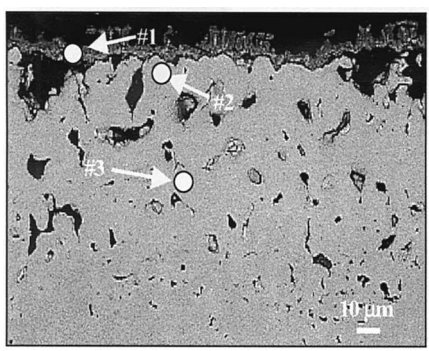

Fig. 9. Inconel 600 coupon after 6-day corrosion at 650°C. Area exposed to gas only. Numbered white spots represent locations of EDS analyses.

Corrosion in the Inconel 625 was similar to that in Inconel 600 in that a corrosion scale developed at the surface and further corrosion occurred deeper in the substrate (Fig. 10). There was a difference, however, in the extent of corrosion between the salt- and gas-exposed regions. The portion of the coupon submerged in the molten salt underwent a noticeable reduction in thickness. In contrast, the corrosion penetration in the Inconel 625 substrate in the gas-exposed area was about 30–70 μm. Most of the weight loss in the Inconel 625 sample was due to mass loss in the submerged region. The corrosion scale in this region, right after the sample was removed from the molten salt, consisted of several layers delaminating from the submerged area and coming together at the salt–gas interface. A spot-chemical analysis was performed on the oxide scale attached to the base metal after cleaning (Fig. 11); the results are given in Table IV. Since molybdenum was one of the elements present in this alloy (9.0 wt.%), the chemical analysis was also run for this element, but no trace was found in the surface

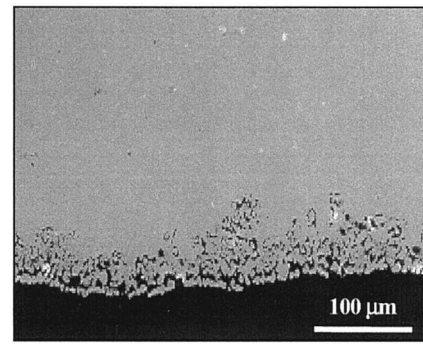

Fig. 10. Inconel 625 coupon after 6-day corrosion at 650°C. Area of coupon exposed to gas only.

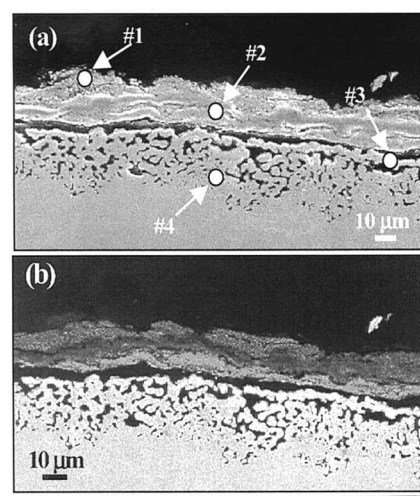

Fig. 11. Inconel 625 coupon after 6-day corrosion at 650°C. Area exposed to gas only. (a) Secondary electron imaging and (b) backscattering electron imaging.

corrosion scale. The XRD results identifying the corrosion products are given in Table III.

It was indicated earlier that in the stainless-steel samples the corrosion was intergranular (Figs. 3 and 4) and that some locations showed conspicuous grain-boundary ditching and grain pullout. It was also observed that the corrosion attack was more intense in the molten salt than in the gas. In the Inconel 600 specimen, on the other hand, the corrosion was transgranular and characterized by an initial pitting at the grain matrix (Fig. 8) that left behind a porous region (Figs. 7 and 8). The Inconel 600 coupon showed similar corrosion attack in the salt- and gas-exposed regions. The corrosion scale was significantly thinner in this alloy.

In contrast, Inconel 625 behaved like the stainless steels, in the sense that the salt-exposed area underwent greater corrosion. The spot analyses

of the corrosion scales for the 316L SS and Inconel 625 specimens show that the distribution of the composition layers in the surface corrosion scale is similar. For instance, the outer-corrosion layer in the 316L SS coupon was enriched in Ni (about 76.6 wt.%) and depleted in Cr (about 5.6 wt.%), while the Inconel 625 showed a similar distribution, that is, 86.2 wt.% Ni, 12.1 wt.% Fe, and 1.7 wt.% Cr. For the Inconel 600 coupon, the outermost layer of the corrosion scale was enriched in Cr. It was not surprising to find that Inconel 625 performed so poorly compared to Inconel 600, since the former contains Mo, a refractory element, which has been found to produce catastrophic corrosion in iron- and nickel-base alloys.[17] On the basis of the information obtained from the EDS and XRD analyses, however, it was difficult to assess the role of Mo curing corrosion.

Interpretation of Results

In our earlier investigation,[9] no corrosion was detected in any of these materials when tested in the lithium chloride salt with pure argon as the cover gas. As reported in this paper, the corrosion was extreme when a cover gas of argon and 10% oxygen was used instead. Even after the test temperature was reduced by 650°C, and the corrosion time was shortened to 6 days, the corrosion was still significant. Clearly, oxygen as gas and not as an oxide plays a critical role in this corrosion. Inconel alloys are known to have better oxidation resistance than stainless steels in other environments and Inconel 600, indeed, showed much better corrosion resistance than the 304 and 316L stainless steels in this study. Inconel 625, on the other hand, experienced greater corrosion than Inconel 600 and the two stainless steels. Note that Inconel 625 contains Mo at levels of 3 to 4.5 times those found in 316L stainless steel (as seen in Table I). Note also, however, that although Mo is present in 316L SS and absent in 304 SS, the difference in corrosion behavior of these two steels was not significant. Apparently, it is not only the presence of Mo in the alloy that makes it susceptible to corrosion in this oxidizing environment with chloride salts, but also the amount of Mn.

Grabke *et al.*[11] in their studies of high-temperature corrosion of steels by chlorine and chlorides, suggest that the oxidation of iron and steel is strongly accelerated by the presence of chlorides. They found $FeCl_2$ at the oxide–metal interface and a porous corrosion scale consisting of Fe_2O_3. Since the scale was not protective, active oxidation takes place. According to their explanation, they formulated a mechanism comprising the following steps: (1) chlorine forms at the corrosion scale surface; (2) the chlorine (or Cl^-) penetrates into the corrosion scale to the oxide–metal interface; (3) formation of chlorides of the alloy components, mostly $FeCl_2$, form and

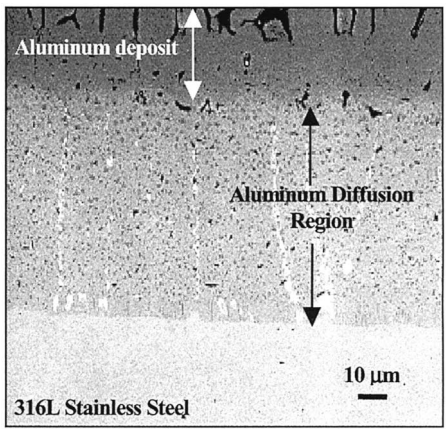

Fig. 12. Aluminized 316L SS after exposure for 30 days at 725°C under reducing conditions (Ref. 2).

continuously evaporate; (4) this chloride is oxidized to Fe_2O_3 and Fe_3O_4 during its diffusion to the outer scale surface, forming a nonprotective scale; (5) the chlorine returns partially to the scale–metal interface. Such a reaction loop exists, in which chlorine acts as a catalyst, accelerating the oxidation.

This mechanism seems somewhat consistent with our results. In our earlier investigation[9] we did not find corrosion when the cover gas was free of oxygen. Such experiments were carried out for 30 days at 725°C. However, in the experiments in which the cover gas also contained oxygen, corrosion was significant even in those samples that were exposed to a lower temperature (650°C) and for just 6 days. It appears that the molten lithium chloride, indeed, was the medium for the oxidation of the materials and for the transport of ions involved in the corrosion and oxidation reactions. It seems that the thin oxide scale that develops in Inconel 625 does not offer much resistance to the diffusion of the chlorine to the oxide–metal interface and to the metal chlorides diffusing back to the surface of the outer oxide scale. In other words, the corrosion mechanism loop described above has a short diffusion path in this last case.

In the discussion of the aluminized stainless-steel coupons, it was noted that the aluminum coating spalled off during testing. No measurable aluminum layer was found in either the immersed or in the gas-exposed region (Ar–10% oxygen) of the coupon. In our previous investigation,[2] the aluminum layer remained attached to the coupon, and it was found that a strong metallurgical bond had developed between the aluminum layer and the metal substrate (Fig. 12). This was caused by the long exposure of the specimen to a temperature of 725°C. An aluminum diffusion region of about 100 μm in the steel coupon is observed. Because aluminizing is conducted

commercially at temperatures of 700–1000°C, it is obvious that the commercially aluminized samples used in the present investigation were not processed properly.

CONCLUSIONS

1. The accelerated corrosion test at 725°C in Ar–10% oxygen gas for 30 days was too severe to assess the corrosion performance of structural materials under conditions expected for a process vessel for treating spent oxide fuels. Tests were then conducted at 650°C for 6 days.

2. On most of the test coupons, the immersed portion experienced the largest corrosion attack. The enhanced corrosion in this region might be due to the presence of the ionic electrolyte that helps in the ionic transfer during the oxidation and corrosion reactions.

3. The 316L and 304 stainless-steel specimens had similar corrosion resistance even with the presence of Mo in the 316L SS. The metal of the welded 316L SS specimen was severely corroded and intergranular attack was detected in the heat-affected zone despite the low carbon content of this steel.

4. The test of the effect of the aluminum coating on the corrosion properties of the 316L SS was inconclusive because the aluminum deposit apparently peeled off due to poor aluminizing processing.

5. Inconel 600 had the best corrosion performance of all the alloys tested. Inconel 625 performed poorly, likely as a consequence of the amounts of molybdenum and chromium present.

ACKNOWLEDGMENTS

This work was performed under the auspices of the U.S. Department of Energy, under Contract No. W-31-109-ENG-38, by the University of Chicago as Operator of Argonne National Laboratory.

The U.S. Government retains for itself, and others acting on its behalf, a paid-up, nonexclusive, irrevocable worldwide license in said article to reproduce, prepare derivative works, distribute copies to the public, and perform publicly and display publicly, by or on behalf of the Government.

REFERENCES

1. C. C. McPheeters, E. C. Gay, E. J. Karell, and J. P. Ackerman. *J. Met.* **49**, 22 (1997).
2. J. E. Indacochea, J. L. Smith, K. R. Litko, and E. J. Karell, *J. Mater. Res.* **14**, 1990 (1999).
3. G. J. Janz and R. P. T. Tomkins, *Corrosion* **35**, 485 (1979).
4. G. Y. Lai, *J. Met.* **43**, 54 (1991).
5. B. W. Burrows and G. J. Hills, *Electrochim. Acta* **15**, 445 (1970).

6. R. L. Every and R. L. Grimsley, *J. Electroanal. Chem. Interfacial Electrochem.* **9**, 165 (1965).
7. D. Inman and M. J. Weaver, *J. Electroanal. Chem. Interfacial Electrochem.* **51**, 45 (1974).
8. M. Takahashi, Y. Katsuyama, and Y. Kanzaki, *J. Electroanal. Chem. Interfacial Electrochem.* **62**, 363 (1975).
9. X. K. Feng and C. A. Melendres, *J. Electrochem. Soc.* **129**, 1245 (1982).
10. A. Rahmel, *Molten salt technology*, D. G. Loverin, ed., Chapter 10 (Plenum Press, New York, 1982), pp. 271–272.
11. H. J. Grabke, E. Reese, and M. Spiegel, *Corros. Sci.* **37**, 1023 (1995).
12. D. Bruce and P. Hancock, *J. Inst. Met.* **97**, 140 (1969).
13. P. Hancock, R. C. Hurst, and R. A. Sollars, *Chemical metallurgy of iron and steel* (The Iron and Steel Institute, London, 1973), p. 415.
14. D. Bramhoff, H. J. Grabke, E. Reese, and H. P. Schmidt, *Werkst. Korros.* **41**, 303 (1990).
15. E. Reese and H. J. Grabke, *Werkst. Korros.* **43**, 547 (1990).
16. E. Reese and H. J. Grabke, *Werkst. Korros.* **45**, 41 (1990).
17. N. Birks and G. H. Meier, *Introduction to high temperature oxidation of metals* (Edward Arnold, New York, 1983), p. 126.
18. O. K. Kotov, *Case-hardening of machine parts by thermo-chemical treatment*, 3rd edn. (Izd-vo Mashinostroenie, Moscow, 1969).
19. *Metals Handbook*, Desk edn., H. E. Boyer and T. L. Gall, eds. (American Society for Metals, Metals Park, Ohio, 1985).
20. W. D. Kingery, H. K. Bowen, and D. R. Uhlmann, *Introduction to ceramics*, 2nd edn. (Wiley, New York, 1976).
21. V. R. Ryabov, *Aluminizing of steel* (Metallurgiya Publ., Moscow, 1973).
22. J. N. Pratt and G. V. Raynor, *J. Inst. Met.*, p. 449 (1951–1952).